sphere ($\psi < 0$) the interference for a positive triplet ($\Phi_\Sigma = 0$) will be constructive ($\hat{\Phi}_\Sigma = 0$). Since the amplitude of the detour excited wave $[\gamma_g(\psi)D_0]$ increases when G approaches the sphere ($\psi \to 0$), the intensity first increases. Then the phase $\hat{\Phi}_\Sigma$ shifts to π and the interference becomes destructive, *i.e.* the intensity drops below the two-beam intensity. With increasing ψ the r.l.p. G leaves the sphere and the amplitude $\gamma_g(\psi)D_0$ of the detour excited wave becomes negligibly small and the observed intensity is that of the two-beam case.

For a negative triplet ($\Phi_\Sigma = \pi$) the situation is completely reversed. When G is outside the sphere ($\psi < 0$) there is no additional phase shift [$\Delta(\psi) = 0$]. Thus $\hat{\Phi}_\Sigma = \pi$, that means the direct and detour excited wave have opposite phases. But for $\psi > 0$ it is $\Delta(\psi) = \pi$ and $\hat{\Phi}_\Sigma = 0$, that means both waves have equal phases. Therefore the observed intensity is first decreased below and then increased above the two-beam intensity level. Hence, comparing the intensity profiles of the same reflection **h** involved in a three-beam case with a positive or negative triplet the following inequalities hold:

$$I_h^+(-\psi) > I_h^-(-\psi); \quad I_h^+(\psi) < I_h^-(\psi).$$

The interference phenomena discussed above give a physical interpretation of some effects contained in the fundamental equations of the dynamical theory. It should be pointed out that the superposition of the exit waves leads to the *Pendellösung* phenomenon and to the spatial distribution of the diffracted intensities within the fan of beams. These effects are not considered in this paper. Whether the intensities of the amplitudes add for the exit beams depends on the choice of the exit boundary conditions (Batterman & Cole, 1964) and therefore on the experimental conditions (*cf.* § 2*c*).

We gratefully acknowledge useful discussions with Professor H. Burzlaff.

References

ALEXANDER, L. E. & SMITH, G. S. (1962). *Acta Cryst.* **15**, 983–1004.

BATTERMAN, B. W. & COLE, H. (1964). *Rev. Mod. Phys.* **36**, 681–717.

BILLY, H. & HÜMMER, K. (1981). *Z. Kristallogr.* **156**, 114.

CHANG, S. L. (1982). *Phys. Rev. Lett.* **48**, 163–166.

CHAPMAN, L. D., YODER, D. R. & COLLELA, R. (1981). *Phys. Rev. Lett.* **46**, 1578–1581.

COLLELA, R. (1974). *Acta Cryst.* A**30**, 413–423.

EWALD, P. P. & HÉNO, Y. (1968). *Acta Cryst.* A**24**, 5–15.

HART, M. & LANG, A. R. (1961). *Phys. Rev. Lett.* **7**, 120–121.

HILDEBRANDT, G. (1967). *Phys. Status Solidi*, **24**, 245–261.

JAMES, R. W. (1948). *The Optical Principles of the Diffraction of X-Rays; The Crystaline State*, Vol. II, pp. 312–315. London: Bell.

KAMBE, K. (1957). *J. Phys. Soc. Jpn*, **12**, 13–31.

KISHINO, S. & KOHRA, K. (1971). *Jpn. J. Appl. Phys.* **10**, 551–557

LAUE, M. VON (1960). *Röntgenstrahl-Interferenzen*, 3rd ed., p. 310. Frankfurt am Main: Akademische Verlagsgesellschaft.

LIPSCOMB, W. N. (1949). *Acta Cryst.* **2**, 193–194.

PINSKER, Z. G. (1978). *Dynamical Scattering of X-rays in Crystals: Solid-State Sciences* 3, edited by M. CARDONA, P. FULDE & H.-J. QUEISSER. Berlin, Heidelberg: Springer Verlag.

POST, B. (1979). *Acta Cryst.* A**35**, 17–21.

Acta Cryst. (1982). A**38**, 848–854

Space-Group Determinations on β- and γ-Brasses

BY P. GOODMAN AND A. J. MORTON

CSIRO Division of Chemical Physics, PO Box 160, *Clayton, Victoria, Australia* 3168

(*Received* 25 *September* 1981; *accepted* 18 *June* 1982)

Abstract

Mixed γ-brass/β-brass samples have been examined by convergent-beam electron diffraction and electron microscopy. This study has led to the allocation of a centrosymmetric space group for the regular inversion antiphase domain superstructure of γ-brass, and also resulted in the identification of a hitherto unreported tetragonal structure for the body-centred cubic ordered β-brass. In the dual convergent-beam/microscopy examination of the γ-brass samples, images were taken from samples thick enough to give structured convergent-beam patterns. The resulting images are complicated by beam convergence to the extent where only the image symmetry can be interpreted directly.

0567-7394/82/060848-07$01.00

Introduction

Electron microscope specimens of Cu-rich γ-brass prepared for study of superstructures of γ-brass (Morton, 1975), were further examined in the JEOL 200CX microscope, and in a Siemens Elmiskop 1 convergent-beam camera fitted with a low-temperature stage (Dowell & Williams, 1976), in order both to inspect the relationship between convergent-beam electron diffraction data and image data for relatively thick foils, and to make space-group determinations.

The method of preparing γ-brass samples from a nominal composition mixture of 50·35 at.% Zn previously reported (Morton, 1974) leads to a matrix of 'normal' β-brass, very close to the stoichiometry CuZn, in which may be found islands having the γ-brass structure with a composition of approximately 57 at.% Zn. In such islands the γ-brass is ordered in a superstructure with periodicity in the present sample of approximately 70 Å. This sample allowed the following symmetry studies.

1. Ordered γ-brass

Inversion and antiphase domains

Two previous studies are relevant to understanding the 'inversion antiphase domain' model for γ-brass. In Morton (1974) long-period superlattices were analysed using bright-field microscopy and selected-area diffraction. The period was found to be composition dependent; in any one *macroscopic* domain the superlattice was found to be purely one-dimensional and parallel to one of the $\langle 110 \rangle$ directions of the γ-brass unit cell (body-centred cubic: $a = 8{\cdot}835$ Å; space group $I\bar{4}3m$). The superstructure within such a region then consisted, to a certain approximation, of microdomain ribbons of 'normal' γ-brass in a regular antiphase domain array (APD structure). The domain boundaries were crystallographic shear planes of a particular type, having finite width and possibly accommodating a higher Cu:Zn ratio than the domains themselves. A second study (Morton, 1975) involving dark-field observations showed further that neighbouring domains formed up–down pairs with respect to the polar axis in the non-centrosymmetric $I\bar{4}3m$ unit cell. These were then properly described as inversion antiphase domains, or IAPD's.

The IAPD model consisted of a regular antiparallel array of supposed cubic γ-brass domains, separated by narrow regions whose detailed structure remained a subject for further study. The present study by convergent-beam diffraction was restricted by the fact that the probe size on the specimen was relatively large, so that it would have been impossible to focus on a single microdomain. Nevertheless, it still seemed worthwhile to examine the patterns obtained with a coarse probe, which would illuminate a large number of microdomains, and also include an appreciable volume of domain boundary material.

Alternative projections

Since the superlattice is formed along only one of the six $\langle 110 \rangle$-type directions of the sublattice, only $\frac{1}{2}$ of the possible [111] orientations, and $\frac{1}{3}$ of possible [100] orientations will show the superperiodicity in the zero-layer diffraction pattern.

When principal projections ([100] or [111] of γ-brass) are found which do *not* contain the long cell edge, *i.e.* projections for which the superlattice row is at some substantial angle to the plane of projection (45 or 54°), we find an almost ideal situation for observing the effects of a three-dimensional or upper-layer interaction in convergent-beam (CBED) patterns. That is, having well-spaced discs corresponding to the sublattice, which do not overlap, we can observe quite dramatic consequences of the inclined 70 Å spacing within those discs. Hence, although the space group of γ-brass is well established as $I\bar{4}3m$, and cubic, we might determine a space group for the superstructure, to see if it agreed with that logically deduced for a coherent structure

The first results are shown in Figs. 1–4. These patterns were taken in the 200CX in the top-entry configuration, and are produced by a relatively large-area (~1000 Å) probe formed by the second condenser lens. The small changes in incident angle needed to excite different reflexions were obtained by manual use of the dark-field tilting coils.

Fig. 1 shows a [111] zone-axis pattern which has hexagonal geometry, but a reduced, $1m$, symmetry due to the ordering along the [101]* direction, out of the plane of the projection. This [101]* vector is coplanar with the mirror line through the pattern and along its $[1\bar{2}1]$* axis. This $1m$ symmetry, evident in a pattern exhibiting strong three-dimensional interaction, which typically reduces the central beam disc to the overall $1m$ symmetry, can be interpreted as corresponding to a mirror plane of the structure.

Fig. 2, in which the $50\bar{5}$ reflexion is directly excited, demonstrates the existence of a diad axis parallel to $[10\bar{1}]$ (and perpendicular to the above mirror plane) by virtue of the internal mirror symmetry of the $50\bar{5}$ disc.

Similarly, Fig. 3 shows a pair of patterns in which the conjugate regions of the $40\bar{4}/\bar{4}04$ reflexions exhibit a pattern identity in an asymmetric intensity distribution. This is a proof for a centre of symmetry (Goodman & Whitfield, 1979) (by chance these patterns were taken across the mirror axis: this does not negate the test, which follows logically from the combination of mirror and diad found in the previous two figures).

This analysis suggests the space group $P2/m$, which is logically consistent with the overall *crystal* symmetry in which the orthorhombic *lattice* symmetry is reduced by parallel but inclined boundaries (see Fig. 4).

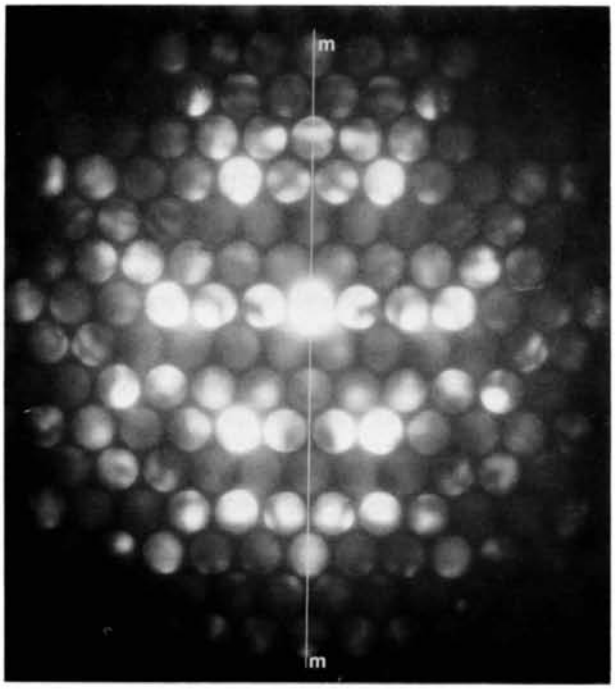

Fig. 1. The [111] zone-axis pattern from a sample of γ-brass, taken in the JEOL 200CX electron microscope at the selected-area diffraction setting. The superlattice vector, indexed as $[101]^*$, lies out of the projection of the figure, but has a projection $[1\bar{2}1]^*$, shown as the line m–m, in the plane of the figure.

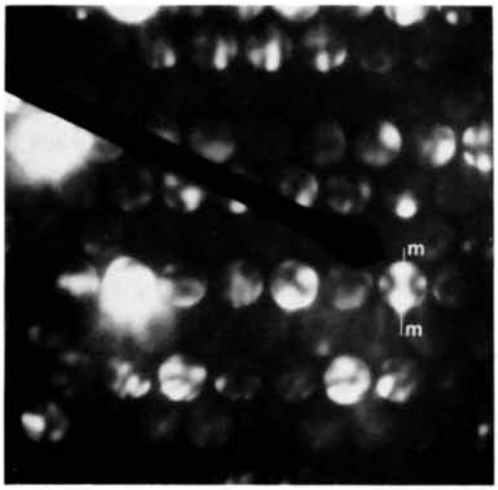

Fig. 2. The pattern obtained from that of Fig. 1 by operating the dark-field-tilt coils so as to excite directly the $50\bar{5}$ reflexion. The $[10\bar{1}]^*$ vector which is the horizontal axis of the pattern, gives the projection axis for the diagram of Fig. 4.

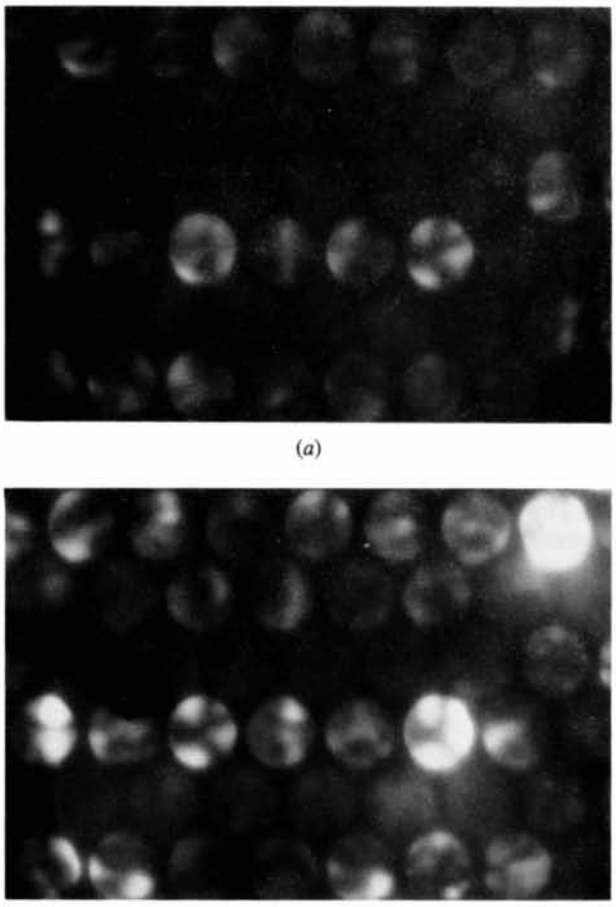

Fig. 3. Obtained as in Fig. 2; the patterns (*a*) and (*b*) show the $40\bar{4}/\bar{4}04$ reflexions respectively displaying equivalent asymmetric patterns, alternatively in (*a*) right-hand field (central row of reflexions) and (*b*) left-hand field (beside the shadowed marker) respectively.

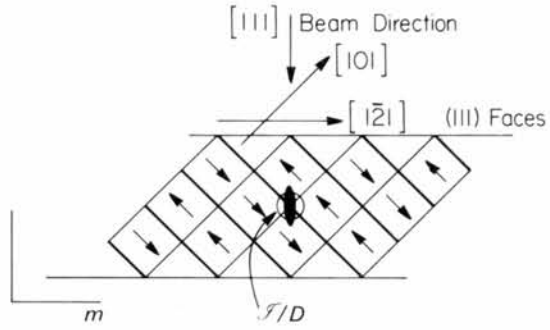

Fig. 4. An idealized model of the antiphase domain structure, shown in $[10\bar{1}]$ projection, with periodicity along [101] and bounded by foil surfaces near (111). I, D and m stand for inversion centre, diad axis and mirror plane respectively. The $[1\bar{2}1]$ vector which is parallel to the $[1\bar{2}1]^*$ vector in Fig. 1 is shown as the projection of the [101] superlattice vector onto the foil surface. Thickened lines (between top and bottom surface) represent domain boundaries.

The same kind of analysis could be carried out for a foil exhibiting (001) boundaries and giving the $1m$ pattern symmetry as in Fig. 5(*b*). Here the mirror plane passes through the [100]* vector of the pattern. This finding of a monoclinic symmetry for the crystal, when the infinitely-extended structure is known to be orthorhombic, means simply, in the case of a parallel-bounded crystal, that we have found a genuine lattice space group, but one appropriate to a larger-than-minimum unit-cell volume.* (This would of course not be true for arbitrarily wedged crystals; hence microscopic polyhedra are not suitable for symmetry work.) It is therefore still a valid aid in structure analysis, particularly when more than one projection is available.

With this in mind it is of interest to confirm the centrosymmetry of the crystal in this new setting. The single pattern of Fig. 6 shows an $hkl/\bar{h}\bar{k}\bar{l}$ translational relationship within the Kossel-line structure, by virtue of having overlapping discs (*i.e.* the zero beam covers both hkl and $\bar{h}\bar{k}\bar{l}$ Kossel bands in one setting) and a strong and distinctive pattern structure.

The overall evidence therefore tends to support the IAPD model (Morton, 1975) for this structure and is consistent with its allocation to the centrosymmetric space group *Pmna* (No. 51) of which $P2/m$ is a subgroup. We do not have enough data however to make the allocation definite. What we have shown to a very high degree of certainty is the existence of a mirror plane in the IAPD structure; it follows therefore that the displacements between domains at the domain boundaries and the domains themselves must conform to this symmetry. To a lesser accuracy we have confirmed a centre of symmetry which must be located in the domain wall.

(*a*)

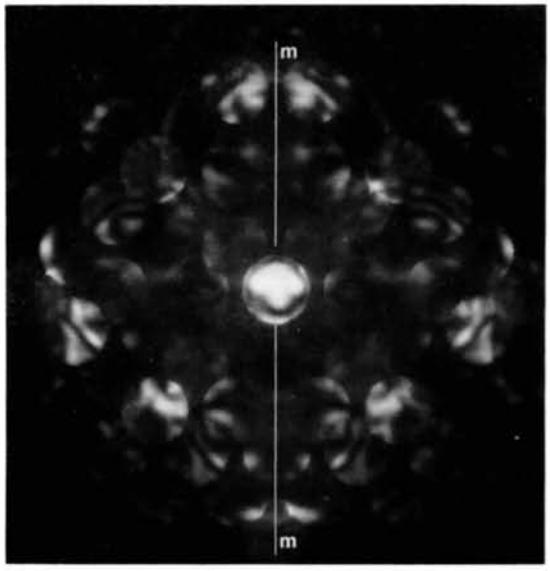

(*b*)

Fig. 5. (*a*) Point pattern from the [001] orientation of γ-brass. The superlattice vector is along the [101]* direction and at 45° to the incident beam direction. (*b*) Convergent-beam pattern from the same region as (*a*) showing $1m$ symmetry.

2. β-Brass: CuZn

Fig. 7 shows the results of examination of the β-brass phase, in the low-temperature convergent-beam

* The authors are indebted to Mr A. F. Moodie for pointing out this elementary fact.

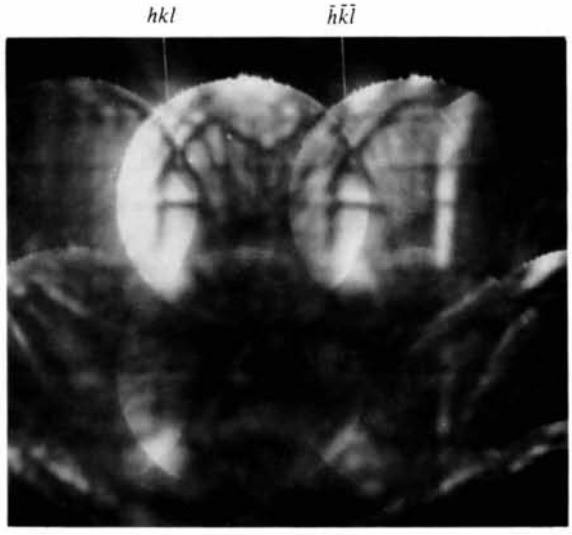

Fig. 6. The simultaneous excitation of an $hkl/\bar{h}\bar{k}\bar{l}$ pair of reflexions, showing a translational relationship of an asymmetric Kossel line pattern.

camera. In Fig. 7(*a*) we recognize the normal β-brass b.c.c. selected-area diffraction pattern, in which weak 100 reflexions (Cu–Zn difference reflexions) appear. This would appear to fit the previously reported and well-known CsCl structure for the ordered phase (a = 2·995 Å; space group: $Pm3m$). However, Fig. 7(*b*), which shows the convergent-beam pattern for the same region at the [001] zone axis, shows a departure from Friedel's law along the [100]* direction, which can only be attributed to the existence of a polar axis. Fig. 8 completes the data with a four-beam pattern, obtained by tilting away from the zone axis so as to excite simultaneously the 200, 110 and $1\bar{1}0$ reflexions. The symmetry components of this pattern are entirely consistent with a structural departure from the CsCl structure by movement of the body-centred atom (Cu) along the [100] direction by a small amount. This would reduce the symmetry to tetragonal, and to space group $P4mm$ (No. 99).

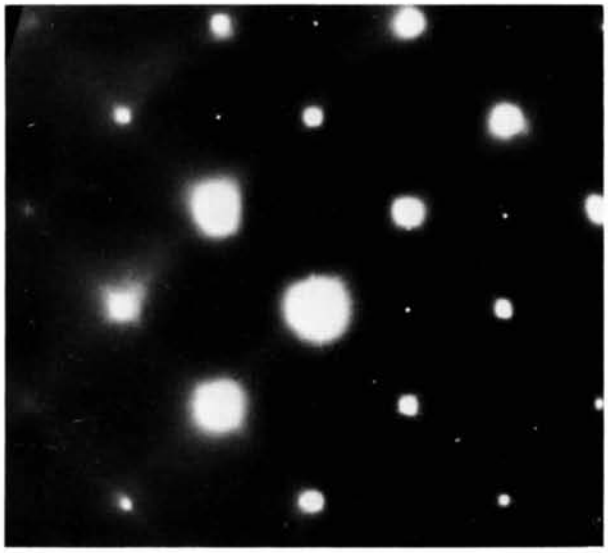

(*a*)

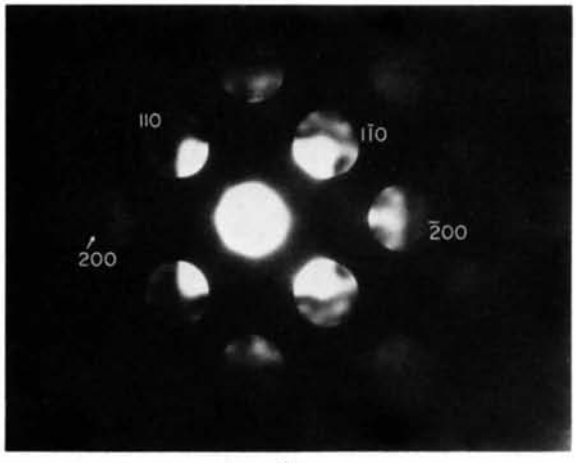

(*b*)

Fig. 7. (*a*) Point pattern from β-brass in the [001] orientation (the very weak difference reflexions, *e.g.* 100, are just visible). (*b*) Convergent-beam pattern from the same region and orientation. Note that 200 and $\bar{2}$00 reflexions, and 110 and $1\bar{1}$0 reflexions, are non-equivalent pairs.

This space group is deduced from the structure model, and no higher symmetry can be allocated to fit the data in view of the cell size. The complementary data of Fig. 8 demonstrates (*a*) the existence of a horizontal mirror plane and (*b*) the existence of a twofold axis parallel to the [100]* vector (this axis is assumed to be a component of the fourfold axis). This is illustrated in Fig. 9. Taken together with the zone-axis pattern of Fig. 7, this removes any ambiguity about the existence of a [100]* polar axis.

The above data were collected at 173 K. We therefore do not know at what temperature a tetragonal → cubic transition occurs. From electron diffraction evidence so far, in fact, it remains an open question as to whether such a transition does occur before the well known order–disorder transition at higher temperatures.

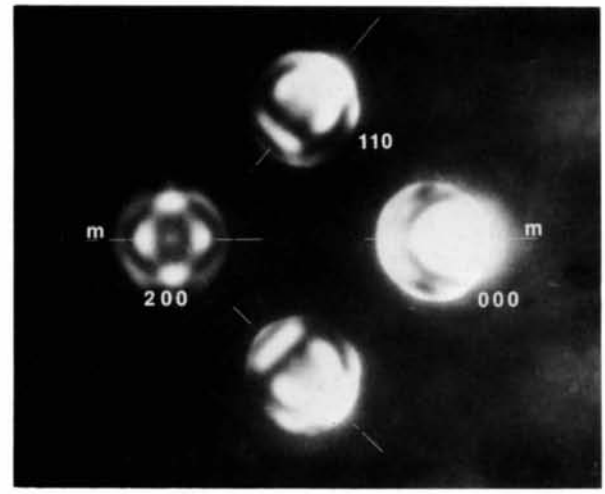

Fig. 8. The four-beam convergent-beam pattern of β-brass with symmetrical excitation of the 200 reflexion.

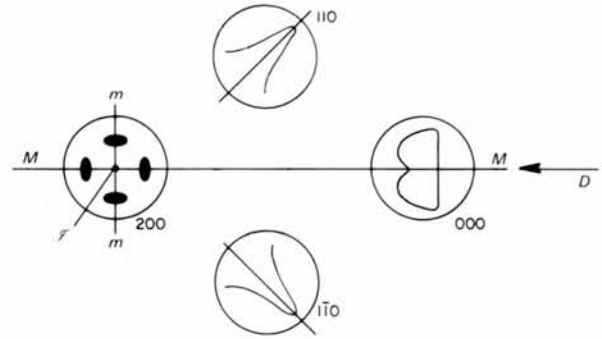

Fig. 9. Diagrammatic representation of the symmetry of Fig. 8. In this figure, M represents a mirror line of the whole pattern, m a mirror line of the 200 disc, $\mathcal{I}$ an inversion centre for that disc, and D is a diad axis for that structure.

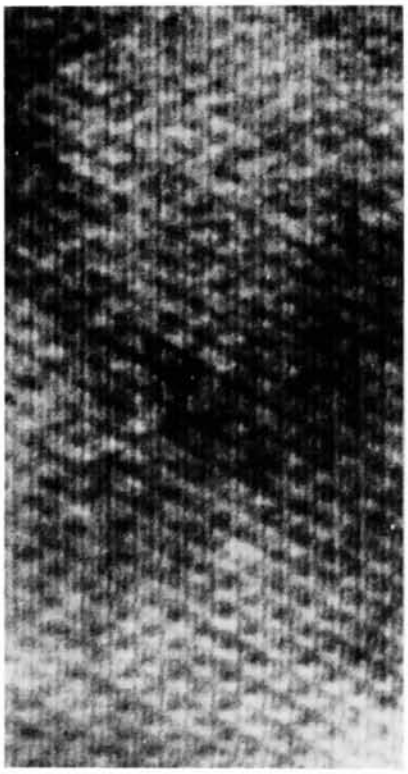

(*a*)

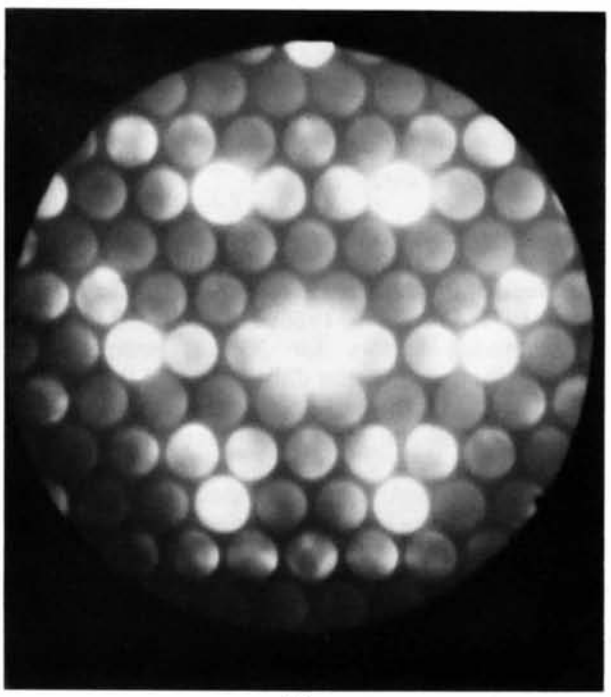

(*b*)

Fig. 10. (*a*) Image from a medium-thick region of γ-brass. (*b*) Diffraction pattern enclosed in the objective aperture, from which the image in (*a*) was taken.

3. Imaging CB patterns

As a further interest, since Figs. 1 and 2 were taken in the back focal plane of the JEOL 200CX high-resolution pole piece, it was decided to examine the image symmetry, as part of an extended study of combined CBED/image-contrast. A zone-axis pattern from a somewhat thinner region than that used for Figs. 1–3 was chosen and enclosed in an objective aperture (Fig. 10*b*). This pattern, however, still shows

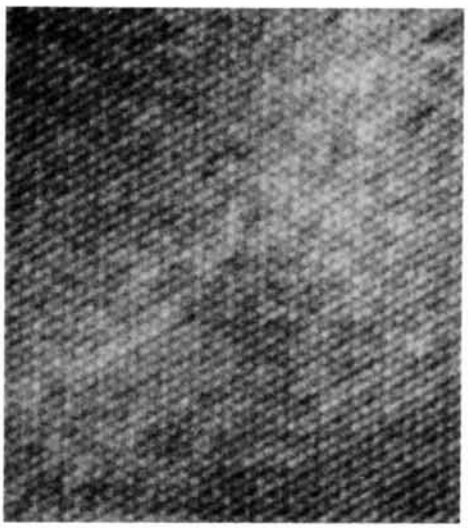

(*a*)

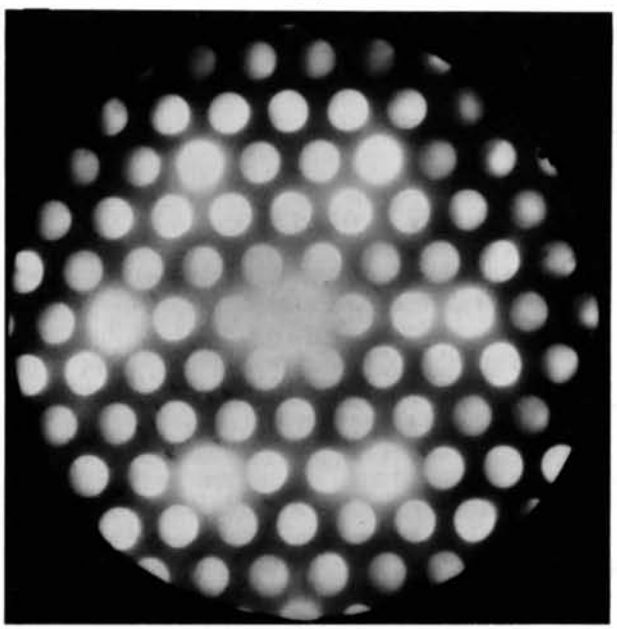

(*b*)

Fig. 11. (*a*) Image from a thinner region of γ-brass showing approximately hexagonal symmetry. (*b*) Diffraction pattern enclosed in the objective aperture from which the iamge in (*a*) was taken.

some CBED contrast, and must be from a medium-thick 200–300 Å region. The lattice image formed from this pattern shows a very marked departure from the hexagonal symmetry shown in the image of Fig. 11(*a*) which was obtained with a much reduced beam convergence (as in Fig. 11*b*) and from a thinner region of the sample. Fig. 10(*a*) shows an image composed of diamond-shaped cells which bear no obvious relationship to a real-space projection. This phenomenon has been reported in summary (Goodman, Moodie, Whitfield, Morton & Rossouw, 1982) but without showing the corresponding diffraction patterns from which the images were obtained. Examination of Fig. 10(*b*) shows that reciprocal space is largely filled with reflexion intensities, due to the high beam convergence, and that we are as much imaging individual reflexions as we are imaging superposed orders in the usual understanding of (parallel illumination) lattice imaging. The superposition of such an amount of angular information must be difficult to interpret except in terms of symmetry, and this is just an extreme example of the phenomenon often noted, that thick-crystal images are difficult to match against those computed, even when beam convergence is taken into the calculation, to some approximation. Fig. 10(*b*) suggests that some of this difficulty must arise from an extreme sensitivity to the precise placement of both the condenser and the objective apertures, as well as to the fact that a substantial background of diffuse intensity fills the region remaining between diffraction orders. It is noted, however, that the crystal region is still substantially thinner than that used for Fig. 1 where there is a marked intensity fringe structure within each disc. It is well known, however, that angular phase modulation appears within the discs at an earlier stage of thickness than that required for intensity modulation.

References

DOWELL, W. C. T. & WILLIAMS, D. (1976). *J. Appl. Cryst.* **9**, 145–158.

GOODMAN, P., MOODIE, A. F., WHITFIELD, H. J., MORTON, A. J. & ROSSOUW, C. J. (1982). *Electron Microscopy and Analysis* 1981. *Inst. Phys. Conf. Ser.* **61**, 271–274.

GOODMAN, P. & WHITFIELD, H. J. (1979). *Acta Cryst.* A**36**, 219–228.

MORTON, A. J. (1974). *Phys. Status Solidi A*, **23**, 275–289.

MORTON, A. J. (1975). *Phys. Status Solidi A*, **31**, 661–674.

Acta Cryst. (1982). A**38**, 854–858

X-ray Debye Temperature for Hexagonal Crystals

BY DAVID SINGH AND Y. P. VARSHNI

Department of Physics, University of Ottawa, Ottawa, Canada K1N 6N5

(*Received* 2 *November* 1981; *accepted* 23 *June* 1982)

Abstract

With the Debye continuum model an analytical expression is derived for the X-ray Debye temperature (θ_M) of a hexagonal crystal in terms of the elastic constants and this expression is used to calculate θ_M for hexagonal crystals of 41 elements and compounds. Calculated results by numerical integration are also presented for the X-ray Debye temperature perpendicular to the hexad axis, $\theta_\perp$, and that parallel to it, $\theta_\parallel$. The calculated results are compared with experimental values, wherever data are available. A correction factor for the effect of dispersion is determined from the experimental data.

Introduction

The Debye–Waller factor is an important parameter in the description of a solid entering into the analysis of numerous solid-state properties (Blackman, 1955; Maradudin, Montroll, Weiss & Ipatova, 1971; Willis & Pryor, 1975; Wertheim, 1968; Lipkin, 1961) including the scattering factors for X-rays, neutrons and electrons (both in electron diffraction and the incoherent scattering of conduction electrons) in addition to the recoilless fraction in Mössbauer experiments.

However, there is a scarcity of experimental data on Debye–Waller factors or equivalently X-ray Debye temperatures in the literature, particularly in the case of non-cubic crystals. This scarcity may be ascribed, at least in part, to the numerous difficulties in the collection and analysis of the appropriate data (Herbstein, 1961), which are compounded for non-cubic crystals by the fact that in such systems the Debye–Waller factors are anisotropic. In the analysis of results based on X-ray and neutron diffraction, corrections are necessary for thermal diffuse scattering. These are complicated by the fact that the thermal diffuse

0567-7394/82/060854-05$01.00